Diamond & Related Materials 30 (2012) 42–47

Contents lists available at SciVerse ScienceDirect

Diamond & Related Materials

journal homepage: www.elsevier.com/locate/diamond

Growth of carbon nanotubes and their field emission pro

Deepak Varshney [a,b,*], Anirudha V. Sumant [c], Brad R. Weiner [b,d], Gerardo Morell [a,b]

[a] Institute of Functional Nanomaterials, University of Puerto Rico, San Juan, PR 00931, Puerto Rico, USA
[b] Department of Physics, University of Puerto Rico, San Juan, PO Box 70377 PR 00936, Puerto Rico, USA
[c] Center for Nanoscale Materials, Argonne National Laboratory, Argonne, IL 60439, USA
[d] Department of Chemistry, University of Puerto Rico, San Juan, PR 00936, Puerto Rico, USA

ARTICLE INFO

Article history:
Received 14 June 2012
Received in revised form 27 September 2012
Accepted 27 September 2012
Available online 5 October 2012

Keywords:
Carbon nanotubes
Diamond
Hot filament chemical vapor deposition
Field Emission

ABSTRACT

Carbon nanotubes (CNTs) have been fabricated on free-standing microcrystalline diamond (FSD) films by hot filament chemical vapor deposition using Ni as catalyst. Micro Raman spectroscopy has been used as a primary technique to characterize the hybrid material, while electron microscopy and electron energy loss spectroscopy served as complementary characterization techniques. The fabricated material shows the presence of multiwall carbon nanotubes of diameters in the range of 10–15 nm with a wall thickness of 5–6 nm protruding from the free-standing microcrystalline diamond films of crystallite sizes ranging from 0.5 to 2.0 μm. The CNT-FSD films show good field emission properties with low turn-on field, large field enhancement factor, and an excellent current stability over a period of 10 days.

1. Introduction

Carbon-based materials, especially graphene, tetrahedrally amorphous carbon (ta-C) films, ultrananocrystalline diamond, carbon nanotubes, and carbon composites are of great interest as electron sources, due to their low threshold emission fields [1–5]. Carbon nanotubes (CNT) have attracted growing interest owing to their unique physico-chemical and mechanical properties leading to their potential applications as electron field emitters for optical displays, micro fabricated X-ray sources, electrode material for fuel cells and lithium ion batteries, and catalyst support, among other applications [6–9].

CNTs have been grown on a variety of materials/substrates such as Cu foils [10], Si wafers [11], and SiC for high temperature devices [12] but their cold cathode application is limited because of their poor resistive contact with the substrate. It has been shown that heat generated at the interface of the CNT film and substrate, due to high joule heating at higher current values near the saturation region [4,13], resulting in various mechanical stresses on the film, which make it difficult to maintain electron emission at low voltage for extended periods of time due to the breakdown of CNTs. The present approach is a step towards overcoming this drawback by fabricating a combination of CNTs and diamond. In such a material, the role of diamond is crucial in enhancing the emission stability of CNTs. Diamond microcrystals help in the process of heat dissipation by acting as efficient heat spreaders that could rapidly transfer heat from devices to sink. Thus, the present material approach would have significant advantage in enhancing the current stability and reproducibility of CNT film which is an important factor for its real life application. CNTs fabricated on free-standing diamond (FSD) films were found to have very high thermal conductivity (~3000 W/km) along with high mechanical compliance and they offer a potential tool for the development of next generation thermal interface materials [14,15].

Here, we report the growth, characterization, and field emission properties of CNTs grown on FSD films. The majority of the synthetic methods for FSD films reported in the literature are directly or indirectly based on processes including chemical etching or mechanical peeling in order to separate the diamond film from the substrate [14] but the present method overcomes the drawbacks of such harsh processes. A structure containing a combination of FSD film for heat spreading and CNTs for current emission could provide a useful combination to efficiently conduct away the heat. The present method is an interesting and scalable technique of fabricating such material in the form of CNT-populated FSD film that can be easily separated from the parent substrate.

2. Experimental procedure

The CNT-populated FSD film was fabricated in a two-step process described below. The first step involved depositing Ni-incorporated FSD films on a Cu substrate followed by CNT growth step.

* Corresponding author at: Department of Physics, University of Puerto Rico, San Juan, PO Box 70377 PR 00936, Puerto Rico, USA.
E-mail address: deepvar20@gmail.com (D. Varshney).

0925-9635 Published by Elsevier B.V. Open access under CC BY-NC-ND license.
http://dx.doi.org/10.1016/j.diamond.2012.09.009

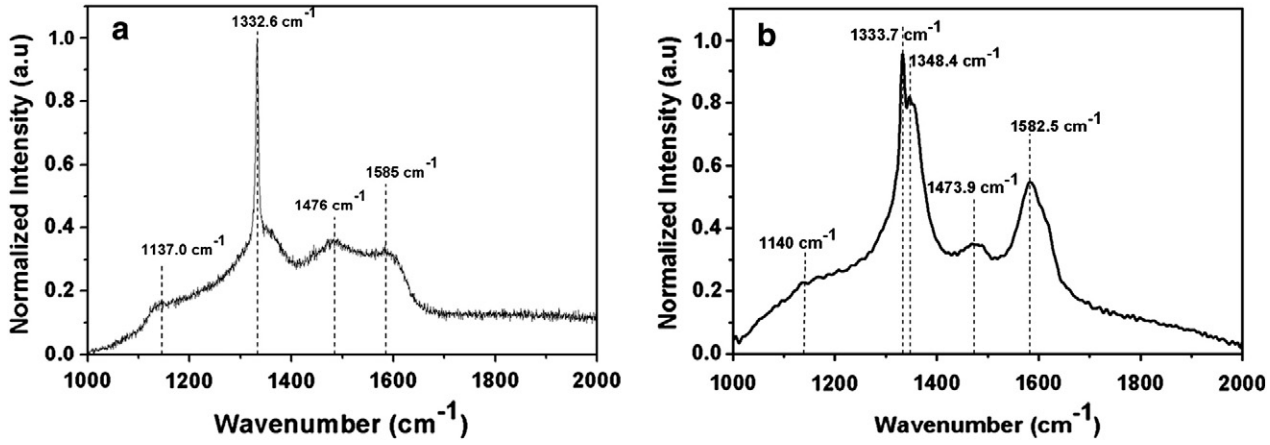

Fig. 1. Raman spectrum of (a) Ni-incorporated FSD prior to MWCNT growth, and (b) MWCNT-populated FSD film showing the characteristic bands of the two carbon materials.

2.1. Ni incorporated free-standing diamond film preparation

Saturated hydrocarbon polymers, n-tetracosane (Alpha Aesar) and n-octacosane (Alpha Aesar) were used during the seeding process. In a typical procedure, 0.05 g diamond powder (Alpha Aesar) and 0.01 g of Nickel nanoparticles of size 20–30 nm (Alpha Aesar) were mixed with 1 g of n-tetracosane and 1 g of n-octacosane and melted on a hot plate by heating the mixture to a temperature of 120 °C at a rate of 15 °C/min. A small portion of this mixture was transferred onto a copper disk substrate (14 mm in diameter) and allowed to cool to room temperature. The disk was then placed in the hot filament chemical vapor deposition (HFCVD) chamber and exposed to a gas mixture consisting of 0.3% methane and 99.7% of hydrogen at a constant pressure of 20 Torr and a total gas flow of 100 sccm. The reaction was activated by a rhenium filament (8 cm in length and 0.5 mm in diameter) positioned at 7.5 mm above the substrate and lasted for 3 h. After the growth, the substrate was allowed to cool down to obtain a Ni incorporated FSD film. After the substrate was cooled down, the film spontaneously detached from the substrate due to the large difference in thermal expansion coefficient of the diamond film and the Cu substrate.

2.2. Carbon nanotube synthesis

The Ni incorporated FSD films were placed in the HFCVD chamber and exposed to a gas mixture consisting of 2% methane and 98% of hydrogen containing 500 ppm of H_2S at a constant pressure of 20 Torr and a total gas flow of 100 sccm at the substrate temperature of 800 °C. The reaction was activated by the filament (2500 °C) positioned at 7.5 mm above the substrate and carried out for 5 min. The resulting material was a CNT-populated FSD film.

The field emission I–V characteristics of the fabricated CNT-populated FSD films were investigated in a custom built system [15].

3. Result and discussion

The Raman scattering spectra of the Ni incorporated FSD and CNT-populated FSD films were obtained on a triple monochromator (ISAJ-Y Model T 64000) with around 1 cm^{-1} resolution using the 514.5 nm line of Ar laser (shown in Fig. 1). Fig. 1a shows the Raman spectrum of a Ni incorporated FSD film, the presence of a band around 1332.60 cm^{-1} confirms the presence of diamond [16], and the band around 1585 cm^{-1} corresponds to G band [17,18]. Also, two more bands around 1160 cm^{-1} and 1480 cm^{-1} are observed, which correspond to the presence of TPA (transpolyacetylene) polymer [18]. The Raman spectrum of the CNT-populated FSD film is shown in Fig. 1b that reveals a sharp and intense peak at 1333.7 cm^{-1} that is a signature of sp^3 bonded C in the diamond phase [16]. The shoulder around 1348.2 cm^{-1} corresponds to the disorder induced in the sp^2 carbon [19]. The band at about 1582 cm^{-1} corresponds to sp^2 hybridized carbon indicating the presence of graphitic carbon [17]. The weak band around 1140 cm^{-1} and a band at 1472 cm^{-1} arise due to the sp/sp^2 bonded carbon which is apparently present in the grain boundaries of the diamond films [20]. The ratio of the intensities of D and G bands is a good indicator of the quality of bulk samples. MWCNT spectrum shows a less intense G band as compared to D band, revealing higher quantity of structural defects due to multiple graphite layers.

The photographic images of the MWCNT-populated FSD film and the Ni incorporated FSD film (Fig. 2) show that the fabricated films are of size comparable to that of copper substrate of 14 mm diameter. After

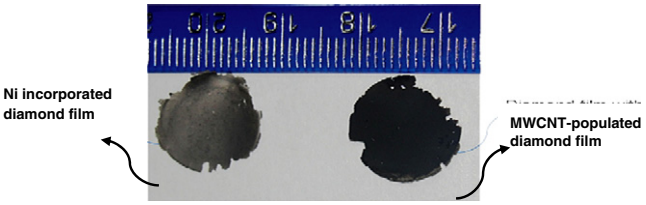

Fig. 2. Photographic image of Ni incorporated FSD film and the MWCNT-populated FSD film.

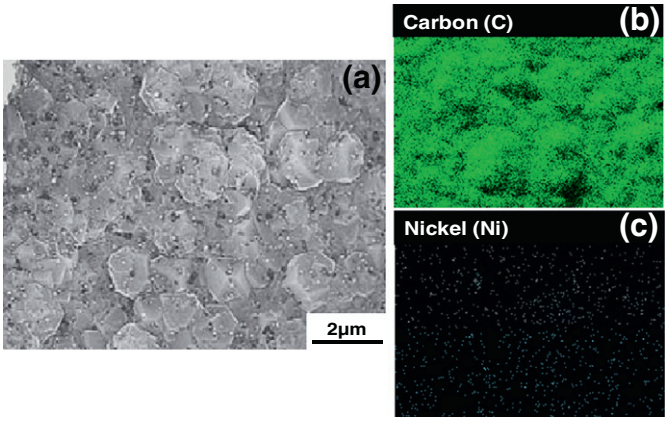

Fig. 3. (a) SEM image of the Ni incorporated free standing diamond film. SEM-EDS mapping of Ni incorporated FSD in the region shown in panel a. (b) Carbon. (c) Nickel.

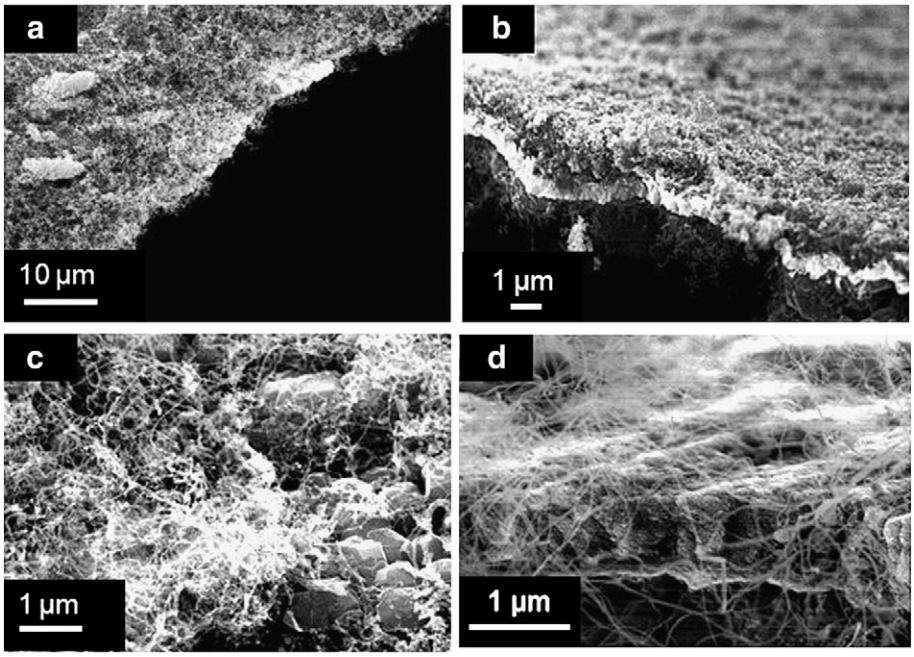

Fig. 4. (a and b) SEM images of MWCNT-populated SSD film, showing CNTs protruding from the diamond microcrystals, (c and d) spread uniformly over it. (e and f) Showing that the thickness of the film is in the range of 1–1.5 μm.

the substrates are cooled down, the films spontaneously detach from the substrates. From the digital image it can be clearly seen that the Ni incorporated FSD film takes a darker tinge after the fabrication of carbon nanotubes indicating high density of MWCNTs on the FSD film.

Fig. 3a shows the SEM image and Fig. 3(b and c) shows the elemental composition mapping of the top surface of the Ni incorporated FSD films prior to CNT growth revealing a uniform distribution of Nickel (Ni) nanoparticles (Fig. 3c) on the diamond surface. The concentration of Ni on the FSD films estimated from energy dispersive spectroscopy (EDS) analyses is around 0.3 at. wt.%.

Scanning electron micrographs (SEM) were recorded using a JEOL JSM-7500F microscope and is used to analyze the morphology of the fabricated material (Fig. 4). Fig. 4a and b shows images of CNTs populated on the FSD films. The FSD films are completely covered with carbon nanotubes despite the high degree of roughness of the diamond film, which is an important factor for improved thermal con-

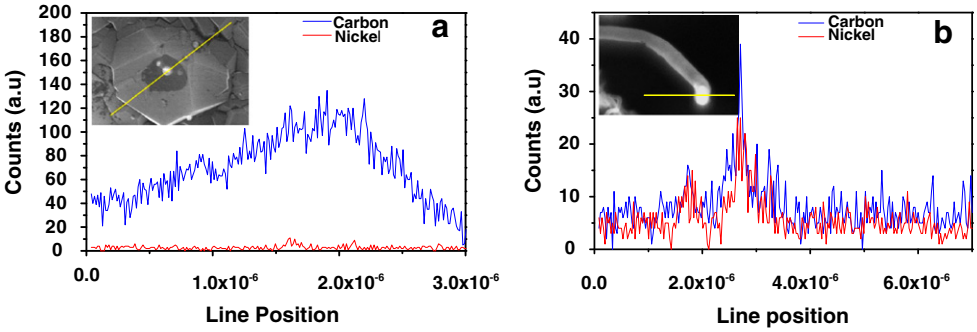

Fig. 5. EDS line spectrum (a) of Ni incorporated FSD films and (b) CNTs with Ni particles at the tip.

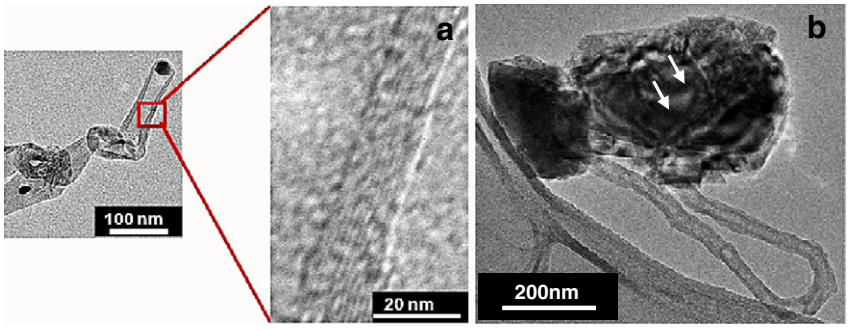

Fig. 6. Transmission electron microscopic image of (a) multiwalled CNT with their wall thickness. (b) Carbon nanotubes bonded with diamond crystals.

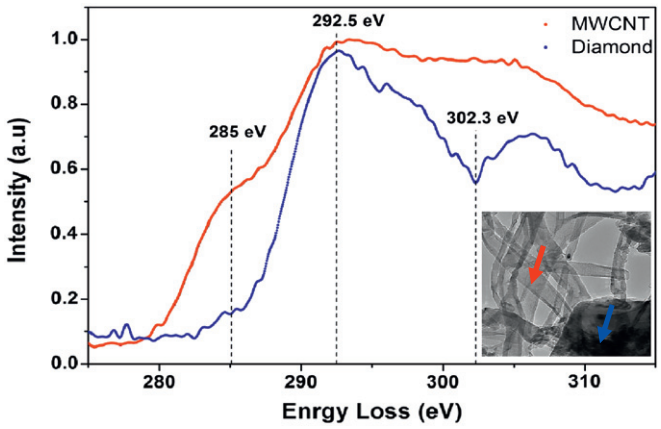

Fig. 7. Electron energy loss spectrum of the region shown in the inset.

tact. It can be seen from the figures that CNTs cover the diamond film like a carpet. Fig. 4c shows the densely CNT-populated microcrystalline diamond films with crystallite sizes ranging from 0.5 to 1.0 μm. Fig. 4d shows the cross-sectional images of the CNT-populated FSD films revealing the thickness of the film to be about 1.0 μm and the length of the tubes to be in the range of 12–20 μm. The SEM-EDX line scan technique was used to detect the distribution of the elements as shown in Fig. 5. The FSD film comprises Ni particles as shown in the inset of Fig. 5a. Fig. 5b shows the line spectrum of the CNTs fabricated on the Ni nanoparticle incorporated diamond films. It reveals the presence of Ni catalyst at the tip of the carbon nanotubes, indicating that the Ni nanoparticles embedded in the diamond film catalyze the formation of MWCNTs and at the same time strengthen the adhesion of CNTs to the diamond film. The prevalence of a tip growth mechanism for CNTs is evident from the high concentration of Ni at the tip.

The CNT-populated FSD films were further analyzed using a Carl Zeiss LEO 922 energy filtered transmission electron microscope (TEM) operated at 200 kV. Fig. 6a shows the multiwalled nature of the CNTs. On further magnification it can be clearly seen that the CNTs consist of ~16 walls. From Fig. 6a it can be seen clearly that carbon nanotubes have a Ni catalyst cap (dark black) at the tip confirming the tip growth mode of tubes which is in agreement with the SEM-EDS line spectra. Fig. 6b shows the presence of diamond particles directly bonded to the CNTs. The appearance of stripes (indicated by arrow) represents the diffraction contour bands, which are indicative of the crystalline nature of diamond [20]. Electron energy loss spectroscopy (EELS) was used to analyze the carbon bonding nature of the carbon material (Fig. 7). EELS has been carried out on different regions of the films, which are shown in the inset of Fig. 7. The EELS spectra recorded on the dark region exhibit distinct and well-established spectral features associated with crystalline sp^3 bonding, the diamond exciton in the range from 289.3 to 293 eV, and the C 1s → σ* transitions around 292.3 eV, which include the second band gap of diamond that produces a pronounced dip at ~302.3 eV. A small peak associated with sp^2 bonding at 285 eV is attributable to the C 1s → π* transition and comes from the sp^2-bonded carbon at the grain boundaries [21]. Also the EELS from the tubular regions show a band around 285 eV which corresponds to the C 1s → π* transition due to the presence of sp^2 hybridized carbon followed with a broader band around 292.3 eV corresponding to the C 1s → σ* transition [22]. The main distinct feature that distinguishes diamond from CNT is the presence of a dip around 302 eV in the diamond spectra, which is absent in the carbon nanotube spectra.

Fig. 8a shows the current versus voltage (I–V) curves of the CNT-populated FSD films at different cathode–anode distances (d_{CA}) from 50 to 200 μm. At each distance, the voltage was raised from zero to a certain value until the emission current reached to 1 mA, and then again decreased to zero. Then the Mo rod was moved to a new distance value from the anode, and the cycle was repeated. The electric field required to produce a current density of 1 nA/cm^2 is known as turn-on field and it was about 198 V for the CNT-FSD film at an anode–cathode distance of 50 μm (shown in Table 1). We can clearly observe (Fig. 8a), as expected, that by increasing the distance d, the turn on voltage increases, and the voltage sweep yields lower field emission currents. The results show that emission current increases rapidly with applied field. The current density exceeded ~1 mA/cm^2 at 2000 V and showed no saturation.

To further understand the emission behavior, the I–V data were analyzed in the light of the classical Fowler–Nordheim theory. Fig. 8b shows the F–N plots resulting from the experimental data of Fig. 8a at varying cathode–anode distances. It is clearly seen from Fig. 8b that for all the d_{CA} values, the presence of two distinct slopes in F–N plot indicates that the electron emission may be due to the different processes like: variation in local density of states at the emitter's tip; solid state transport; interaction among adjacent tubes and adsorption/desorption of gaseous species even under high vacuum conditions due to emission-assisted surface reaction processes [23–28]. Also, it may be due to the sharp rings formed by electrons emitted in the thermal-field regime away from apex of hot nanotubes [29]. The presence of sp^2 hybridized carbon around the grain boundaries of diamond film also plays an important role in field emission from the diamond film. The sp^2 graphitic carbon phases present in the grain boundary areas serve as electron transport channels in the surface field emission process [30]. An increase in local temperature

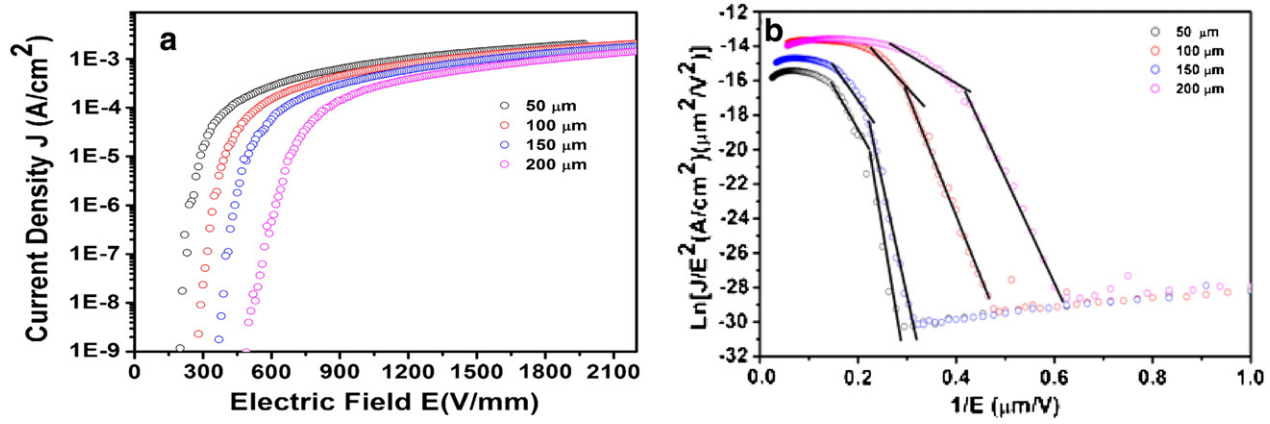

Fig. 8. Field emission properties of the fabricated material (a) current as a function of applied voltage. (b) The corresponding Fowler–Nordheim ($\ln(I/V^2)$ vs E^{-1}) plot.

Table 1
Turn on field at different cathode–anode distances, field enhancement factor at high and low field regime and the local electric fields for the present material.

Cathode–anode distance (d_{CA})	Turn on voltage(V)	Enhancement factor (β)		Local electric field E_L (V/nm)
		At high field(β_H)	At low field(β_L)	
50	198	~10^4	~10^2	3.99–12.39
100	288	~10^4	~10^2	2.36–6.63
150	370	~10^3	~10^2	2.83–14.53
200	490	~10^3	~10^2	2.84–14.20

at the grain boundaries results in the increase in number density of electrons that enhances the emission yield. On the other hand, an increase in the distance (d_{CA}) results in a decrease in temperature leading to an increase in potential barrier for electron tunneling thus weakening the field emission [30,31]. The slope in the high field region is much lower than that in the low field regime. The field enhancement factor β can be calculated from the slope of the F–N plot using an expression,

$$\beta = \frac{B\phi^{3/2}d}{slope} = \frac{-\left(6.83\times10^3\right)\phi^{3/2}}{slope}$$

where, B is a constant that is equal to -6.83×10^3 V(eV)$^{3/2}$ (μm)$^{-1}$, d is the distance of the anode from the emitting surface. Assuming that the work function of CNTs is close to that of graphite (4.5 eV) [32], β was calculated to be in the range of 1.23×10^4–1.0×10^2 for distances from 50 to 200 μm. The high values of β (Table 1) signify that the local electric field is very high at the tip of the CNTs, resulting in the tunneling of electrons from the Fermi level to the vacuum, through potential barrier [33,34]. The improved field emission properties are related to the sharp tips and better crystalline geometry which enhances the local electric field at the tip of MWCNTs. Furthermore, the adequate population density of CNTs on the FSD films also contributes to the low turn-on field and high β value by decreasing the screening effects in the field emission process and thus facilitating the emission of electrons at the applied field.

One important issue to be addressed in case of CNT-based emitters is emission stability and lifetime. Although CNT has very high thermal conductivity, in the absence of better heat sink, most of the heat gets dumped at the CNT/substrate interface leading to the destruction of emission sites. The long-term emission stability of the CNT populated FSD films was measured at a constant field of 5 V/μm and is shown in Fig. 9. The CNTs showed stable emission properties without degradation during continuous operational time of more than 10 days. The observed results are compared with the previous reports shown in

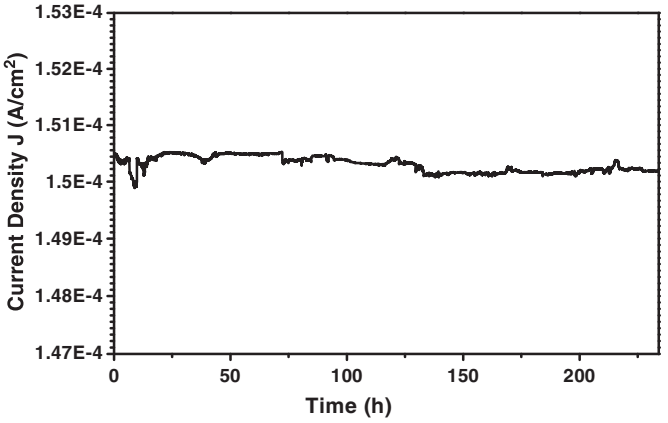

Fig. 9. Results of the field emission current stability test.

Table 2
Comparison of field emission properties of pure carbon nanotubes with present material.

Reference	Turn on field (V/μm) for d_{CA} = 100 μm	Field enhancement factor	Current stability (min)
[36]	1.88–2.22	10^3–10^4	240
[37]	3.0	10^4	180
[38]	~1	10^4	1240
[39]	0.5–0.7	10^3–10^4	960
Present work	3.0	10^2–10^4	>14,000

Table 2 revealing excellent emission stability. We believe that the prolonged stability is due to the presence of diamond, well bonded at the interface, which removes the excess heat, maintaining the integrity of the emission sites [35], resulting in much improved field emission current stability.

4. Conclusion

MWCNTs were successfully fabricated on Ni incorporated FSD films by hot filament chemical vapor deposition using a novel approach. The material exhibits enhanced emission properties as compared to CNTs (multi-walled or single-walled) alone, with the advantage of improved reproducibility and long term stability. This improvement might be ascribed to the seamless integration of CNTs on FSD films, leading to the effective removal of heat at the CNT/diamond interface; thus avoiding the insidious heating effects that prevent the wider use of CNTs as a cold cathode material.

Acknowledgments

This research was made possible by funds from the Institute for Functional Nanomaterials (NSF Grant # 1002410), PR NASA EPSCoR (NASA Cooperative Agreements # NNX07AO30A and NNX08BA48A), and PR DOE EPSCoR (DOE Grant # DEFG02-08ER46526). We would like to acknowledge the help of Mr. W. Pérez with the Raman spectroscopy measurements and Mr. Frank Mendoza with the SEM measurements. Use of the Center for Nanoscale Materials was supported by the U.S. Department of Energy, Office of Science, Office of Basic Energy Sciences, under Contract No. DE-AC02-06CH11357.

References

[1] O. Auciello, A.V. Sumant, Diamond Relat. Mater. 19 (7–9) (2010) 699.
[2] D. Varshney, V.I. Makarov, P. Saxena, A. Gonz'alez-Berr'ıos, J.F. Scott, B.R. Weiner, G. Morell, Nanotechnology 21 (2010) 285301.
[3] D. Varshney, C.V. Rao, M.J.-F. Guinel, Y. Ishikawa, B.R. Weiner, G. Morell, J. Appl. Phys. 110 (2011) 044324.
[4] D. Varshney, B.R. Weiner, G. Morell, Carbon 48 (2010) 3353.
[5] N.A. Monteiro-Riviere, A.O. Inman, Y.Y. Wang, R.J. Nemanich, Nanomed. Nanotechnol. Biol. Med. 1 (2005) 293.
[6] R.H. Baughman, A.A. Zakhidov, W.A. Zakhidov, Science 297 (2002) 787.
[7] R.S. Ruoff, D.C. Lorents, Carbon 33 (1995) 925.
[8] S. Iijima, Nature 354 (1991) 56.
[9] S. Iijima, T. Ichihasi, Nature 363 (1993) 603.
[10] B.A. Cola, X. Xu, T. Fisher, Appl. Phys. Lett. 90 (2007) 0935131.
[11] J. Xu, T. Fisher, Int. J. Heat Mass Transfer 49 (2006) 1658.
[12] J. Bonard, C. Klinke, Phys. Rev. B 67 (2003) 115406.
[13] K. Kordas, G. Toth, P. Moilanen, M. Kumpumaki, J. Vahakangas, A. Uusimaki, R. Vajtai, P.M. Ajayan, Appl. Phys. Lett. 90 (2007) 1231051.
[14] C. Varanasi, J. Petry, L. Brunke, B.T. Yang, W. Lanter, J. Burka, H. Wang, J.S. Bulmer, J. Scofield, P.N. Barnes, Carbon 48 (2010) 2442.
[15] G. Morell, A. Gonzalez-Berrios, B.R. Weiner, S. Gupta, J. Mater. Sci. Mater. Electron. 17 (2006) 443.
[16] In: J.E. Field (Ed.), The Properties of Diamond, London Academic Press, 1979, p. 325.
[17] A.R. Badzian, T. Badzian, R. Roy, R. Messier, K.E. Spear, Mater. Res. Bull. 23 (1988) 531.
[18] A.C. Ferrrai, J. Robertson, Philos. Trans. R. Soc. Lond. A 362 (2004) 2477.
[19] W. Kalss, R. Haubner, G. Lippold, B. Lux, Diamond Relat. Mater. 7 (1998) 158.
[20] A.C. Ferrari, J. Robertson, Phys. Rev. B 63 (2001) R121405.
[21] D. Varshney, V.I. Makarov, P. Saxena, J.F. Scott, B.R. Weiner, G. Morell, Eur. Phys. Lett. 95 (2011) 28002.

[22] J.E. Butler, A.V. Sumant, Chem. Vap. Deposition 14 (2008) 145.
[23] J.M. Lee, J.S. Park, S.H. Lee, H. Kim, S. Yoo, S.O. Kim, Adv. Mater. 23 (2011) 629.
[24] J.M. Bonard, J.P. Salvetat, T.R. Stockli, W.A. de Heer, L. Forro, A. Chatelain, Appl. Phys. Lett. 73 (1998) 918.
[25] R.B. Rakhi, K. Sethupathi, S. Ramaprabhu, Nanoscale Res. Lett. 2 (2007) 331.
[26] C. Dong, M.C. Gupta, Appl. Phys. Lett. 83 (2003) 159.
[27] K.A. Dean, B.R. Chalamala, Appl. Phys. Lett. 76 (2000) 375.
[28] P.G. Collins, A. Zettl, Phys. Rev. B. 55 (1997) 9391.
[29] M. Marchand, C. Journet, C. Adessi, S.T. Purcell, Phys. Rev. B. 80 (2009) 245425.
[30] Y.L. Li, J.J. Li, Q. Wang, C.Z. Gu, Diamond Relat. Mater. 18 (2009) 229.
[31] S.K. Srivastava, V.D. Vankar, D.V.S. Rao, V. Kumar, Thin Solid Films 515 (2006) 1851.
[32] Y. Wei, C. Xie, K.A. Dean, Appl. Phys. Lett. 79 (2001) 4527.
[33] S. Suzuki, C. Bower, O. Zhou, Appl. Phys. Lett. 76 (2000) 4007.
[34] R.C. Smith, J.D. Carey, R.D. Forrest, S.R.P. Silva, J. Vac. Sci. Technol., B 23 (2) (2005) 632.
[35] T. Connolly, R.C. Smith, Y. Hernandez, Y. Gun'ko, J.N. Coleman, J.D. Carey, Small 5 (7) (2009) 826.
[36] R.B. Rakhi, K. Sethupathi, S. Ramaprabhu, Carbon 46 (2008) 1656.
[37] R.B. Sharma, D.J. Late, D.S. Joag, A. Govindaraj, C.N.R. Rao, Chem. Phys. Lett. 428 (2006) 102.
[38] S.H. Lim, H.S. Kim, C.H. Lee, S.M. Pietruszko, J. Jang, J. Non-Cryst. Solids 299–302 (2002) 864.
[39] W.Y. Sung, J.G. Ok, W.J. Kim, S.-M. Lee, E.Y. Jang, Y.H. Kim, Nanotechnology 18 (2007) 335705.